Complementary projector for null-space stiffness control of redundant assembly robot arm

Nikola Lukic and Petar B. Petrovic
Department for Production Engineering, University of Belgrade, Faculty of Mechanical Engineering, Belgrade, Serbia

Abstract

Purpose – Stiffness control of redundant robot arm, aimed at using extra degrees of freedom (DoF) to shape the robot tool center point (TCP) elastomechanical behavior to be consistent with the essential requirements needed for a successful part mating process, i.e., to mimic part supporting mechanism with selective quasi-isotropic compliance (Remote Center of Compliance – RCC), with additional properties of inherent flexibility.

Design/methodology/approach – Theoretical analysis and synthesis of the complementary projector for null-space stiffness control of kinematically redundant robot arm. Practical feasibility of the proposed approach was proven by extensive computer simulations and physical experiments, based on commercially available 7 DoF SIA 10 F Yaskawa articulated robot arm, equipped with the open-architecture control system, system for generating excitation force, dedicated sensory system for displacement measurement and a system for real-time acquisition of sensory data.

Findings – Simulation experiments demonstrated convergence and stability of the proposed complementary projector. Physical experiments demonstrated that the proposed complementary projector can be implemented on the commercially available anthropomorphic redundant arm upgraded with open-architecture control system and that this projector has the capacity to efficiently affect the task-space TCP stiffness of the robot arm, with a satisfactory degree of consistency with the behavior obtained in the simulation experiments.

Originality/value – A novel complementary projector was synthesized based on the adopted objective function. Practical verification was conducted using computer simulations and physical experiments. For the needs of physical experiments, an adequate open-architecture control system was developed and upgraded through the implementation of the proposed complementary projector and an adequate system for generating excitation and measuring displacement of the robot TCP. Experiments demonstrated that the proposed complementary projector for null-space stiffness control is capable of producing the task-space TCP stiffness, which can satisfy the essential requirements needed for a successful part-mating process, thus allowing the redundant robot arm to mimic the RCC supporting mechanism behavior in a programmable manner.

Keywords Robotic assembly, Complementary projector, Null-space stiffness, Redundant robot arm

Paper type Research paper

1. Introduction

Any physical interaction of robot with its environment (constrained motion) is predominantly defined by the stiffness (or compliance) properties of the robot arm mechanism and the elastomechanical properties of the environment. Compliance of the robot arm mechanism can be modified and controlled. This is fundamentally important because, in executing tasks with constrained motion, robot arm and its environment are two coupled dynamic systems (Hogan, 1985), whereby the robot must adjust its dynamics, primarily its compliance, to the elastomechanical properties of the environment, which as a rule cannot be influenced. Two research aspects are relevant in this context:

1. compliance as a feature of safety and backdrivability in collaborative systems, which involve physical human–robot interaction (pHRI), where there are no exact requirements, and the key priority is that the control system achieves sufficient compliance and stability of the robot system as a whole; and
2. compliance as a process variable, where the need for precise shaping of compliance parameters emerges as the basic requirement, depending on the requirements imposed by the successful execution of a specific task.

One of the considerations in this paper are certain aspects of the compliance control of the robot arm mechanism as a process variable. Compliance as a process variable is encountered in a broad class of industrial tasks, primarily in part mating (Chen *et al.*, 2009; Wang *et al.*, 2015), which is distinct in its extraordinary complexity, but also in deburring, polishing (contour following), screwdriving, machining, et cetera (Huang *et al.*, 2016; Kazerooni, 1988). In addition to the technological tasks, precise compliance control is of generic importance for other fields of robotic technology application as well, for example in medicine, in the field of rehabilitation (Zhou *et al.*, 2014) or surgery (Sanan *et al.*, 2014), needle

The current issue and full text archive of this journal is available on Emerald Insight at: **www.emeraldinsight.com/0144-5154.htm**

Assembly Automation
39/4 (2019) 696–714

[DOI 10.1108/AA-10-2018-0163]

This research work is supported by the Serbian Ministry for Education, Science and Technology Development through the project titled Smart Robotics for Customized Manufacturing, grant no: TR35007.

Received 22 October 2018
Revised 10 March 2019
Accepted 1 April 2019

insertion into soft tissue (Dedong *et al.*, 2012) and ultrasound diagnostics (Petrovic *et al.*, 2014; Salcudean *et al.*, 1999). A similar situation is also encountered in the field of service robotics, where there is also a requirement for precise compliance control (Dietrich *et al.*, 2011; Ott *et al.*, 2017; Vukobratovic and Borovac, 2004).

The research topic of compliance as a process variable in this report is limited to robotic assembly and the part mating task in precise mechanical assemblies (for example, engines and similar assemblies in automotive industry). This operation is complex and consists of:

- primary task – achieving required relative position and orientation of the mating parts, as well as the trajectory of their relative motion (insertion trajectory); and
- secondary task, which is comprised of compensation for the ideal mating trajectory deviations, that is, for dynamic compensation for relative position and orientation error.

The theory of assembly of compliantly supported rigid parts, the foundations of which were laid as far back as the 1970s and 1980s (Nevins and Whitney, 1977; Whitney, 1982) and later gradually refined and revised (Ciblak and Lipkin, 1996; De Fazio *et al.*, 1984; Southern and Lyons, 2002), defines the necessary compliance properties, which ensure a successful assembly process. A practical implication of this theory is the Remote Center of Compliance unit (RCC), whose passive mechanical structure is designed to ensure the properties of physical compliance are consistent with a successful assembly process (Whitney, 1982). However, although the RCC unit and the entire theory of quasi-static assembly of compliantly supported rigid parts has been fully confirmed experimentally, wider practical application in the industry has not taken place, primarily because of the problem of inherent inflexibility. The RCC unit is always tightly tailored for specific application, which is directly opposite to the new paradigm of mass customization production systems, which require extreme flexibility and diversification (Jovane *et al.*, 2003). Additionally, there are other drawbacks, systemic in nature.

In the context of robotized assembly, when a robot as a universal manipulation system also executes the process of part mating, the application of compliantly supported rigid parts theory starts from the assumption that the robot arm mechanism is an infinitely stiff system. This assumption is unsustainable because each of the robot joints possesses certain compliance, thus providing overall robot arm compliance as observed relative to task-space. In this manner, compliance of the entire assembly system changes its character. This problem has been long-recognized, along with its consequences (De Fazio *et al.*, 1984). However, instead as an indeterminate source disturbing the overall elastomechanical behavior of the assembly system, robot arm compliance can be observed as a programmable source of compliance, which is the focus in this paper. The above-stated poses two fundamental questions on:

- the task of producing desired overall stiffness as a programmable process variable consistent with the theory of assembly of compliantly supported rigid parts in specific application (is it possible and how?), which solves the problem of flexibility; and
- the issue of potential conflict between the motion control task and the compliance control task, that is, the issue of uniting and achieving complementarity between the primary and secondary task comprising the assembly operation.

Authors of this paper look for a potential answer to these questions in applying increased mobility in the case of kinematically redundant robot arm, where it is possible to execute internal motion, which does not affect the position of the robot arm TCP. In this way, unlike classical, widespread and broadly applied non-redundant robots, with the ability of executing only single tasks, redundant robots are able to execute multiple tasks simultaneously if the concept of prioritization is introduced. Theoretical framework for kinematic redundancy control represents an approach based on the well-founded mathematical apparatus of linear algebra (Lay, 2005; Yanai *et al.*, 2011).

The concept of control based on task prioritization was first formally posed in (Liegeois, 1977), and the following systematic approaches to control of the mechanism of kinematically redundant robot arm in (Baillieul *et al.*, 1984). Generalization of this approach, including the analysis of kinematic and algorithmic singularities, is presented in (Siciliano and Slotine, 1991), with extensions (Baerlocher and Boulic, 2004). In addition to kinematic aspects, modelling dynamic behavior bears high importance in this context (Khatib, 1987; Nakamura *et al.*, 1987), encompassing active force control in conditions of constrained robot arm motion with fundamental formulations (Khatib, 1995), which laid the foundation for further for breakthroughs and application in modern research. Current research of this topic, although mainly focused on service robotics and related operations, deals with and resolves significant general theses such as collision avoidance in interaction with environment (Dietrich *et al.*, 2012), achievement of motion within pre-set speed and acceleration limits (Flacco *et al.*, 2015), avoidance of singular configuration of the robot arm, task hierarchy control, including stability aspects (Dietrich *et al.*, 2015), and null-space compliance (Karami *et al.*, 2018). One of the approaches in this field also refers to the development of bio-inspired methods and derived algorithms (Leylavi *et al.*, 2016). Very significant results of research into compliance of robot arm mechanism, including control aspects, were presented in (Kim *et al.*, 1992; Salisbury, 1980), especially for the case of redundant robots (Albu-Schaffer *et al.*, 2004; Ott, 2008; Svinin *et al.*, 2002), with special regard to the influence of the robot arm configuration on the elastomechanical behavior of the TCP (Ajoudani *et al.*, 2015). However, what has not been the subject of deeper analyses, and is still a topic insufficiently explored, with especially prominent absence of physical verification, is relating the fundamental task of TCP position motion control to the simultaneous control of the task-space TCP compliance properties by applying task prioritization based on kinematic redundancy (primary and secondary tasks), where compliance is considered a process variable with precisely defined requirements and parameters.

Based on the requirements for successful execution of the precise part mating process and the possibility of its implementation on kinematically redundant anthropomorphic robot arm, in this paper we present the results of years of

research conducted at CyberManufacturing Systems Laboratory with the following main goals:

- transferring compliance properties of the RCC unit to the robot arm mechanism with the performance required for precise mechanical assembly;
- achieving flexible compliance and implementing the concept of "programmable RCC," possessing the ability to instantly adjust to the needs of the process; and
- practical test of the developed theoretical models and, especially, exact quantification of the achieved robot arm compliance performance and the results of implementing the primary task of robot motion in task-space.

Methodological approach is based on:

- mathematical apparatus of linear algebra and, in that framework, synthesis of the complementary projector, mathematically consistent with simultaneous execution of the primary task of robot motion and achievement of required compliance within the configuration null-space of the kinematically redundant robot arm mechanism;
- application of the open-architecture control system and kinematically redundant industrial robot, which is basically a conventional, commercially available industrial robot, whereby the practical verification is conducted on a physical platform, which is completely identical to the real-world conditions of industrial application and which allows simple practical implementation; and
- development and application of the appropriate methodology for experimental physical identification and verification of the achieved elastomechanical behavior of the robot arm under very delicate metrology conditions – stiffness performance is difficult to measure, especially because of the strong effect of frictions, which exist in the actuation mechanism of each joint.

The paper is organized in four chapters. Following the introductory part, in the second chapter we present the analysis of the elastomechanical behavior of the robot arm and the theoretical approach of synthesis of isotropic compliance complementary projector. Results of practical verification, which encompassed a computer simulation and a physical experiment, are presented in chapter three. Chapter four includes a discussion of the obtained results and a definition of possible improvement and future research directions.

2. Null-space projector for compliance control

2.1 Basic requirements for part mating process – quasi-isotropic compliance

Part mating process is fundamentally a contact process. In high precision loose fittings, clearance is 0.01 mm, which is at least one order of magnitude smaller than the accuracy of positioning and following a programmed trajectory of an industrial robot (typically around 0.10 mm or poorer). Consequently, even in the case of ideally positioned parts, errors resulting from inherent imperfection of robot arm mechanics and control system, inevitably cause their collision. Constrained motion of this type is essentially different from most other (for example, machining process or writing on board) in its indeterminability, which is a consequence of accidental and non-stationary character of the mentioned positioning error. At the same time, in precision metal assembly, whose elements most commonly feature high rigidity and surface hardness (heat treated steel), contact forces are of great magnitude with a prominent dynamic component, equally in the orthogonal and the tangential plane. Especially critical is the friction phenomenon, which, owing to its inherently non-linear properties, in this context results in the appearance of two distinctive states of interaction of parts in the process of assembly: jamming and wedging (Whitney, 1982). In both cases, the process of assembly, that is, the relative motion of the parts being assembled, instantaneously stops, thus forcing the entire system for robotic part mating to go into an irregular state, regardless of the intensity of the force applied. This is why the compliant behavior of the robotic mechanism is a categorical imperative for successful execution of this task.

However, compliance in itself is not sufficient. In a general case, compliance of arbitrary properties does not have the tendency to take the robot system out of the irregular state such as jamming and wedging.

As mentioned in the introductory part, the RCC unit possesses the properties of physical compliance consistent with a successful assembly process. Essentially, the RCC unit possesses the property of mechanical isotropy (force excitation causes translatory displacement as a response, while the response to torque excitation is rotary displacement), whereby both cases provide collinearity of corresponding excitation vectors and response vectors. In addition, the RCC unit achieves the previously stated properties of compliant support at a fictive point in space, the compliance center, whose location is determined by the adopted parameters of its mechanical structure. It is important to emphasize that the location of the compliance center can be arbitrarily chosen. This further implies that it can be located, that is, projected outside the physical envelope of the RCC unit (this is where Remote Center of Compliance comes from). The concept and principle of the RCC unit are illustrated in Figure 1, with an additional photo of a physical implementation example (Petrovic, 1988).

The baseline for analysis of the elastomechanical behavior of the compliant support system (robot and/or RCC) is represents by a fundamental relation which connects the excitation force vector $F \in R^{m}$ with response in the form of an infinitesimal displacement $\delta x_F \in R^{m}$ (in the process of assembly, excitation is represented by the generalized contact force vector emerging from part collision):

$$F = K_x \delta x_F = K_x (X_0 - X) \tag{1}$$

Matrix function of mapping force to the displacement is represented by the generalized stiffness matrix $K_x \in R^{mxm}$, where m is the number of the degrees of freedom in the task-space, whereby the elastomechanical behavior of the structure or mechanism considered in the kinetostatic domain is defined entirely by the values of its elements (task-space TCP stiffness), Figure 2.

Considering the applicative context where the anthropomorphic robot arm is used as manipulation system to perform part mating tasks in assembly technology, it can be concluded that shaping the generalized stiffness matrix, i.e.

Figure 1 RCC unit – structure, operating principle (simplified concept, true behavior/shape follow beam elastic neutral axis deflection according to Euler–Bernoulli beam equation) and example of physical implementation

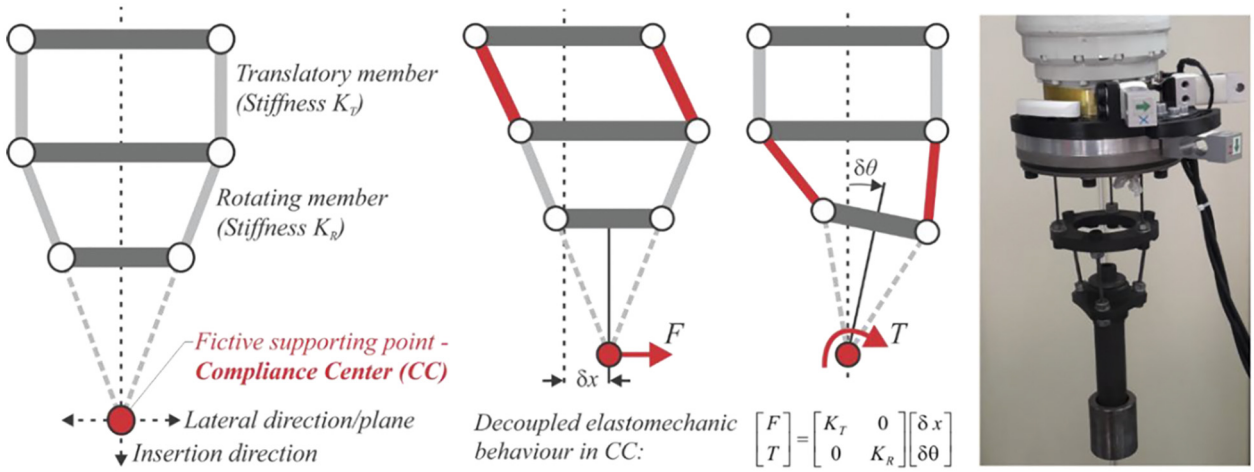

task-space TCP stiffness matrix, of its mechanism can achieve the desired elastomechanical behavior of the robot arm. In this paper, the focus is on finding the conditions under which the robot arm mechanism and its actuation system can produce the desired matrix shape K_x, in such a way as to define stiffness/compliance as process variables. In the specific case of part mating, the task is to achieve programmable elastomechanical isotropy – "programmable RCC".

For further analysis of the possibility to achieve previously stated requirements, below we consider the aspects of mapping robot arm joint stiffness to the task-space TCP stiffness. Joint stiffness of the robot arm is represented by the joint-space stiffness matrix $K_q \in R^{nxn}$, where n is the number of the degrees of freedom of the robot arm. Observation of the serial kinematic structure, whereby it is considered that compliance is concentrated in the rotary joints of the robot arm, yields the conclusion that task-space TCP stiffness K_x represents the resulting stiffness and that it is the consequence of the actuation mechanism stiffness of each joint and robot arm configuration. Accordingly, it is not possible to directly shape matrix K_x, but it is possible to do it indirectly by shaping matrix K_q, practically $K_x = f(K_q)$, thus making mapping between joint and task-space

Figure 2 Reduction of robot arm mechanism stiffness to equivalent generalized spring with 6 degrees of freedom in the general case – 3 translations and 3 rotations: m = 6 → $X \in R^{6\times 6}$ and $K_x \in R^{6\times 6}$, (Petrovic and Lukic, 2017)

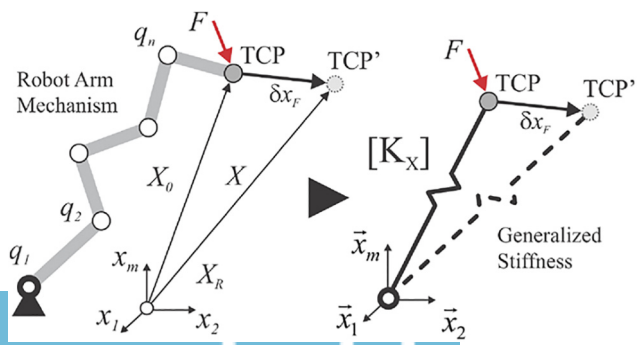

TCP stiffness the fundamental basis for finding a solution in achieving the desired elastomechanical behavior of the redundant robot arm mechanism.

2.2 Joint to task-space stiffness mapping for redundant robot arm

Establishing a correlation between joint and task-space TCP stiffness is achieved by mapping the external excitation force vector $F \in R^m$ to the actuation torques vector $\tau \in R^n$ in the joints of the robot arm, by applying the virtual work principle (Craig, 2005). Neglecting gravitation and friction member, differentiation of the actuation torques vector with respect to the joint coordinates of the robot arm mechanism $q \in R^n$ results in direct derivation of the joint-space stiffness matrix $K_q \in R^{nxn}$:

$$K_q = -\frac{\partial \tau}{\partial q} = -\frac{\partial}{\partial q}\left[\mathcal{J}^T(q) K_x \delta x_F\right] = \mathcal{J}^T(q) K_x \mathcal{J}(q) - \left[\frac{\partial}{\partial q}\mathcal{J}^T(q)\right] K_x \delta x_F \quad (2)$$

When the second element in the relation (2) is disregarded, considering that the infinitesimal displacement of the robot arm TCP in task-space is $\delta x_F \approx 0$, the joint-space stiffness matrix is reduced to a congruent transformation of the following form (Salisbury, 1980):

$$K_x \to K_q(q, K_x) = \mathcal{J}^T(q) K_x \mathcal{J}(q), \; K_q \in R^{n\times n} \quad (3)$$

By applying congruent transformation (3), upon mapping it to the configuration space of the robot arm, the desired shape of the task-space TCP stiffness matrix K_x is transformed to the joint-space stiffness matrix K_q whose off-diagonal elements do not equal zero in a general case. Presence of off-diagonal elements is a consequence of the mathematical nature of congruent transformation (3). However, the problem emerges once it is required to physically implement the joint-space stiffness matrix K_q, which is off-diagonal and corresponds to the desired shape of the task-space TCP stiffness matrix K_x.

Generally, the solution to this problem can go along two directions:

1 polyarticular actuation – single actuator drives multiple joints, most often two, which can directly generate off-diagonal elements of the matrix K_q. This type of solution is encountered in biological systems (human arm). However, in the technical sense, such a solution is extremely complex for physical implementation; and
2 existence of kinematic redundancy of the robotic mechanism, where the joints are mutually independently driven, which takes the complexity to the area of mathematical modelling and an attempt to synthetize an adequate control algorithm.

In this paper, search for a solution to the problem of the existence of off-diagonal elements of joint-space stiffness matrix K_q, as a consequence of congruent transformation, is focused on the second stated option, that is, on the efficient use of increased mobility present in the case of kinematic redundancy of the robot arm in relation to the task-space ($r = n\text{-}m \geq 1$).

The most common case in practice, which refers to the process of part mating, is that the desired task-space TCP stiffness matrix K_{xd} has diagonal shape, and that its off-diagonal elements equal zero. Such shape of the task-space TCP stiffness matrix provides decoupled elastomechanical behavior of the robot arm, which is consistent with the compliance properties of a passive support system (RCC unit), which ensures successful performing of the part mating process, achieving the following exact requirements:

- quasi-isotropy, which results in the response vector of the robot arm, displacement δx, having the same support, i.e. being collinear with excitation force vector F, whereby the intensity of the displacement vector of the robot arm TCP in task-space directly depends on the value of the main diagonal elements of the matrix K_x, and in relation to that; and
- selective compliance, where the values of the main diagonal elements are defined so that compliance is lower in the direction of the parts being mated, and higher in the lateral plane.

The character of the elastomechanical behavior of the robot arm TCP is represented by a stiffness ellipsoid in 3D, or a stiffness ellipse in 2D space, which can also be used as an indicator of the extent to which the desired compliance properties have been achieved. The stiffness ellipsoid can be constructed based on the calculated eigenvectors v and eigenvalues λ of the task-space TCP stiffness matrix K_x, which defines the orientation of the principal ellipsoid axis and the values of its semi-axes. Relation of the matrix $K_x \in R^{mxm}$ to eigenvalues and eigenvectors is expressed as:

$$K_x v_i = \lambda_{xi} v_i \rightarrow \begin{bmatrix} k_{x11} & \cdots & k_{x1m} \\ \vdots & \ddots & \vdots \\ k_{xm1} & \cdots & k_{xmm} \end{bmatrix} \begin{bmatrix} v_{1i} \\ \vdots \\ v_{mi} \end{bmatrix} = \lambda_{xi} \begin{bmatrix} v_{1i} \\ \vdots \\ v_{mi} \end{bmatrix}, \quad i = \overline{1,m} \tag{4}$$

Figure 3 Character of elastomechanical behavior of the robot arm TCP ($q \in R^3, x \in R^2$) presented by the stiffness ellipse

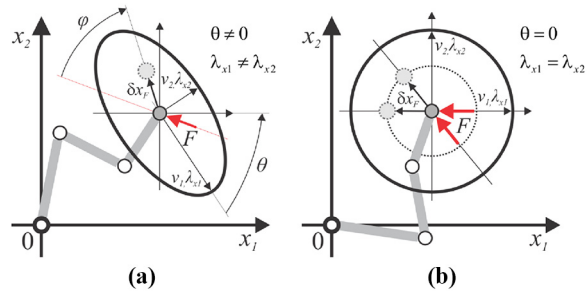

Notes: (a) General case; (b) case of isotropy – ideally from the aspect of the assembly process (RCC)

Two characteristic cases of elastomechanical behavior represented by the stiffness ellipse, for a planar model of the robot arm mechanism ($q \in R^3, x \in R^2$), are shown in Figure 3.

Figure 3a shows a general case when $\lambda_{x1} \neq \lambda_{x2}$. Ellipse axes in the general case are not parallel to the axes of the arbitrarily selected coordinate system of the task-space. Here the response vector, displacement δx_F, is not collinear with the excitation force vector F, except in the case when vector F is collinear with the major or minor axis of the stiffness ellipse. Angle φ represents the extent of collinearity and it is calculated based on the scalar product and norm of vectors of the excitation force F and response δx_F:

$$\varphi = \arccos\left(\frac{\vec{F} \cdot \overrightarrow{\delta x_F}}{||\vec{F}||\,||\overrightarrow{\delta x_F}||}\right) \tag{5}$$

In the special case, Figure 3b, when $\lambda_{x1} = \lambda_{x2}$ the ellipse is transformed into a circle and then the compliance properties of the robot arm mechanism in the task-space x_1x_2 are isotropic, that is, the angle φ always equals zero. Isotropy is a desirable property because, in the case of precise assemblies, collinearity of the excitation vector F and the response vector δx guarantees to compensate in an optimal way for errors in the positioning of the parts being mated. Otherwise, there is a possibility of producing a new error, of a less favorable character than the initial. The property of collinearity is of essential importance for the efficiency of the RCC unit in practical application.

The key issue is whether and to what extent the shape of matrix K_x can be controlled by changing the configuration of the redundant robot arm through efficient use of increased mobility, as was previously proposed, to achieve the desired elastomechanical behavior in the way that partially or fully emulates the behavior of RCC. If this can be accomplished, considering that the robot is a programmable machine, then it is possible to generate an RCC unit of flexible, controllable/programmable properties by using the robot arm mechanism.

2.3 Complementary projector

Inverse kinematic transformation represents the basic relation required for the implementation of any control law of the robot arm mechanism motion. Unlike the widely applied non-redundant robots, inverse kinematic transformation in

kinematically redundant robots, as linear algebra explains (Lay, 2005; Yanai *et al.*, 2011), consists of two displacement components of joint coordinates as:

1 those that produce correspondent motion of the robot TCP in task-space, which we call particular component δq_P; and
2 the so-called homogenous component δq_N which produces zero displacement in the robot TCP, that is, it produces motion of the robot arm mechanism in the configuration null-space, i.e., in the null-space of the Jacobian matrix $\mathcal{J}(q) \in R^{mxn}$ (Baillieul *et al.*, 1984):

$$\delta q = \delta q_P + \delta q_N = \mathcal{J}^+(q)\delta x + P^c_{N(\mathcal{J})}\delta q_0 = \mathcal{J}^+(q)\delta x + \left[I_n - \mathcal{J}^+(q)\mathcal{J}(q)\right]\delta q_0 \quad (6)$$

where $\delta x \in R^m$ and $\delta q \in R^n$ are infinitesimal displacement vectors in the task and configuration space, respectively, $\mathcal{J}(q) \in R^{mxn}$ rectangular Jacobian matrix, and $\mathcal{J}^+(q) \in R^{nxm}$ its generalized inversion (Moore–Penrose pseudoinversion), then $\delta q0$ in the general case represents an arbitrary displacement vector of the joint coordinates of the robot arm mechanism, while matrix $[I_n - \mathcal{J}^+(q)\mathcal{J}(q)]$ represents a complementary projector denoted by P^c, which vector δq_0 projects in the null-space of the Jacobian matrix $\mathcal{J}(q)$, where I_n is the identity matrix $I \in R^{nxn}$. Moore–Penrose pseudoinversion is one of the possible solutions for calculating the inversion of the rectangular Jacobian matrix, and it is expressed as follows:

$$\mathcal{J}^+(q) = \mathcal{J}^T(q)\left[\mathcal{J}(q)\mathcal{J}^T(q)\right]^{-1} \in R^{n\times m} \quad (7)$$

In the infinite field of possible solutions to inverse kinematic transformation of the redundant robot arm, this solution meets the condition of the minimum norm of the joint coordinates displacement vector. Moore–Penrose pseudoinversion lowers the degree of complexity and it is favorable from the aspect of numerical calculations, but as this solution is not unique, there is room for further improvement in this context (Dietrich *et al.*, 2015).

Presence of the homogenous component δq_N in expression (6) is the consequence of redundant degrees of freedom in relation to the number of the degrees of freedom required to execute manipulation task (n-$m \geq 1$), which allows for the execution of internal motion of the robot arm mechanism, which does not affect the tracking of the desired trajectory of the robot arm TCP. Such higher degree of mobility in executing manipulation task with primary status allows the introduction of a secondary task (Petrovic and Lukic, 2017; Siciliano and Slotine, 1991) within which it is then possible to meet the additional requirements fully or partially, depending on the specific case of application. In the case of part mating process, it is required to enable the execution of the secondary task of the desired TCP elastomechanical behavior through synthesis of the complementary projector $P^c\delta q_0$, which will generate the homogenous component δq_N in the displacement model (6) and in the ideal case, considering the classification in Figure 3, provide the state of mechanical isotropy or a compromise solution by relaxing the requirements. This represents the foundation for establishing the relation between the configuration null-space and compliance of the robot arm mechanism in task-space. In the general case, the search for the solution takes place in the complete task-space or in one or more of its subspaces.

Referring to previous considerations and bearing in mind relations (3) and (7), it is obvious that joint-space stiffness matrix K_q is a function of joint coordinates, and thus any internal motion, which can be executed in the configuration null-space, implicitly has an effect on the change in the shape of the task-space TCP stiffness matrix K_x:

$$K_x(q, K_q) = \mathcal{J}^{+T}(q)K_q\mathcal{J}^+(q), \; K_x \in R^{m\times m} \quad (8)$$

The above said yields a potential possibility within the framework of the secondary task that a robot arm configuration could be selected, from the set of possible solutions, consistent with the diagonal shape of the joint-space stiffness matrix and complementary with the execution of the primary task of achieving the desired position of the robot arm TCP. This can be done by establishing an adequate objective function $u = u(q, K_q(K_{xd}))$ and its gradient vector $\delta qc = \nabla(u)$.

2.4 Quasi-isotropic compliance complementary projector

Building on the previous propositions regarding the formulation of the desired elastomechanical behavior of the robot arm, it is important to emphasize that this context encompasses two related requirements. The first requirement results from the part mating process and refers to generating the desired task-space TCP stiffness matrix K_{xd} as a process variable in task-space. The second requirement is connected to the first through transformations (3) and (8), and refers to the achievement of corresponding joint stiffness in the configuration space presented by the matrix $K_q = f(q, K_{xd})$. Therefore, in this paper the focus is placed on shaping the joint-space stiffness matrix K_q as an object of optimization to attain its physically achievable, diagonal shape. Accordingly, the objective function for indirect minimization of discrepancy between the real and desired task-space TCP stiffness of the robot arm is defined using the Euclidian norm of the off-diagonal elements of the joint-space stiffness matrix K_q (Petrovic and Lukic, 2017):

$$u(q, K_{xd}) = \|k_{q\_ij}(q, K_{xd})\|_{\left[\frac{n(n-1)}{2}\right]} = \sqrt{\sum_{i=1}^{m-1}\sum_{j=i+1}^{n}\left(k_{q\_ij}(K_{xd}, q)\right)^2} \quad (9)$$

Rather than particularly minimizing each off-diagonal element of K_q separately, by introducing their norm, the search for the optimal solution is drastically simplified mathematically, which bears great importance from the aspect of practical application in the control of task-space TCP stiffness matrix K_x of the robot arm in real time. In addition, the approach of summary observation of the off-diagonal elements of matrix K_q, although at first arguable, because it closes insight into their individual values, does not pose any practical risk because off-diagonal elements cannot be physically produced in non-redundantly actuated robots. They are pure mathematical abstraction, produced by congruent transformation (3), they do not exist in the physical domain, and therefore their individual values bear

no significance. Still, this attitude should not lead to the wrong conclusion because they do have significant implications for the task-space TCP stiffness K_x.

By applying the gradient method to the objective function (9), which forms the scalar potential field in the configuration space of the robot arm, it is possible to generate the displacement vector of joint coordinates δq0=δqc, and further synthesize the isotropic compliance complementary projector of the kinematically redundant robot arm as a homogenous component of the generalized displacement model (6), in the following form:

$$P^c_{IC}(q) = \delta q_N = P^c_{N(\mathcal{J})}(q) \cdot \delta qc = \left[I_n - \mathcal{J}^+(q)\mathcal{J}(q)\right]\left(\frac{\partial}{\partial q}u(q)\right) \tag{10}$$

2.5 Possible implications and limitations

Isotropic compliance complementary projector (10), defined analytically, generates a displacement vector component of the joint coordinates, corresponding to the secondary task, disregarding the kinematics of the primary task. Owing to this fact, disproportionate particular and homogenous components of the generalized displacement model (6) can appear which can potentially lead to disturbance in the execution of the primary task caused by null-space motion. Consequently, we propose to introduce a control parameter in the following form (Petrovic and Lukic, 2017):

$$\alpha = \gamma \frac{\|\delta q_{Pi}\|}{\|\delta q_{Ni}\|}, \quad \gamma > 0 \tag{11}$$

Parameter α in the general sense represents a control parameter of vector δqc intensity and the homogenous components δq_N in the displacement model (6). Observation of the task hierarchy as a whole yields the conclusion that such choice of parameter α for the proposed projector (10) provides an adequate relative relation in executing the tasks of primary (δq_P) and secondary (δq_N) hierarchical level, such that the vector intensity of the execution of the set of secondary tasks is proportionate to the vector intensity of the primary task execution, where γ is the global multiplier whose value is determined at higher levels of control.

In accordance with this, the reformulated form of the isotropic compliance complementary projector that includes control parameter can be expressed as follows:

$$\begin{aligned} P^c_{IC}(q) = \delta q_N &= \alpha \cdot P^c_{N(\mathcal{J})}(q) \cdot \delta qc \\ &= \alpha \cdot \left[I_n - \mathcal{J}^+(q)\mathcal{J}(q)\right]\left(\frac{\partial}{\partial q}u(q)\right) \end{aligned} \tag{12}$$

Alternatively, as opposed to the control parameter (11), a categorical condition can be introduced in the form of hard limit, the choice of which can ensure kinematic and dynamic consistency. In this case, by defining the maximum allowable value δq_{Nmax} of the homogenous component δq_N produced by the isotropic compliance complementary projector, the following is true:

$$\delta q_N = \begin{cases} P^c_{IC}(q) & if \ \|P^c_{IC}(q)\| \le \delta q_{Nmax} \\ \dfrac{\delta q_N}{\|\delta q_N\|}\delta q_{Nmax} & if \ \|P^c_{IC}(q)\| > \delta q_{Nmax} \end{cases} \tag{13}$$

Categorical limitation (13) has no effect on the achieved performance of the robot arm TCP null-space stiffness, but only on the convergence speed towards the optimal value of the objective function (9).

Reformulated projector (12) and introduction of the stated limitations still do not encompass some very important aspects of the primary and secondary task realization in the physical domain, such as avoidance of singularity zones or certain types of saturation.

Previously posed questions and perceived opportunities for the enhancement of the isotropic compliance complementary projector can potentially be implemented within the framework of expanding tasks on the secondary hierarchical level by assigning a set of non-process criteria. By defining additional criteria, efficient use of increased mobility and motion control in the configuration null-space of the kinematically redundant robot arm could encompass the limitations with respect to joint displacement of the robot arm, speed, acceleration, actuation torques, etc. An integrated approach in implementation and monitoring of multiple task execution on the secondary hierarchical level could be achieved by introducing a null-space observer, which would contain an adequate inference engine for intelligent decision-making. This issue is not explored in this paper, but it is very important as it would allow avoiding intuitive or trivial solutions.

3. Experimental verification

Verification of the synthesized projector (12) is based on the minimalist approach and conducted on a redundant robot with minimal configuration for the case of two-dimensional task-space (m = 2→$x \in R^2$). Minimal configuration in this case is represented by an anthropomorphic planar mechanism with three DoF (n = 3 → $q \in R^3$), one of which is redundant, i.e. r = n−m = 1 (Figure 4).

Elastomechanical behavior of the adopted minimal configuration is represented by the joint-space stiffness matrix

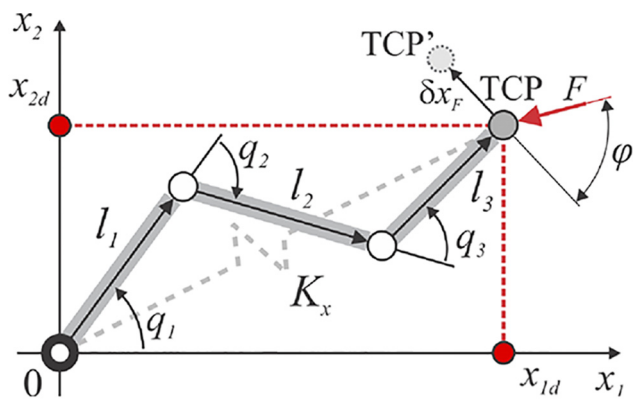

Figure 4 Planar mechanism of the kinematically redundant robot arm ($q \in R^3$, $x \in R^2$ – three-dimensional configuration space and $x \in R^2$ – two-dimensional task-space), whose elastomechanical properties in the task-space are determined by the stiffness matrix $K_x \in R^{2\times 2}$

Notes: Angle φ (5) is the collinearity measure of the excitation force vector $F \in R^2$ and response vector $\delta x_F \in R^2$

$K_q \in R^{3\times 3}$ (3) in the configuration space and the task-space TCP stiffness matrix $K_x \in R^{2\times 2}$ (8) in the task-space (TCP stiffness). Matrix K_x in the general case contains off-diagonal, that is, cross-coupling elements.

To eliminate the direct effect of the gravitation member and thereby preserve the analytical correctness of the model defined by relation (2), 2D task-space and the configuration of the planar robot mechanism were chosen so as to be orthogonal to the gravitation acceleration vector g.

Projector (12) verification was conducted as a simulation and physically, with the following task structure:

- primary task – maintaining the desired initial TCP position, that is, $x(t) = x_d \in R^2$; and
- secondary task – achieving the desired stiffness properties $K_x(t) \to K_{xd} \in R^{2\times 2}$

The generalized displacement model of the robot TCP (6) yields the conclusion that in this case the displacement of joint coordinates degenerates on the homogenous component, that is $\delta q = \delta q_N = P^c_{IC}(q)$. Such composition of the task creates specific conditions in the complete robot configuration space, which allow the system to be monitored under the sole influence of the synthesized isotropic compliance complementary projector (12). None of this, naturally, reduces the functional role of the mechanism of the primary and secondary task fusion, because even passive TCP also produces motion and inevitably generates changes in the entire robot configuration space.

Verification was conducted for two variant parameters of the previously set task: CASE#1 and CASE#2 (Table I). The basic difference is in the subspaces of the robot arm configuration space. Configuration subspace is determined by the desired coordinates of the TCP in the task-space xd (primary task), which is why in this specific case the subspaces chosen were those characteristic for the execution of the part mating task in robotic assembly. The set of initial joint coordinates of the robot arm mechanism q_{in} is selected arbitrarily, but so as to be consistent with x_d (q_{in} is the joint coordinates vector in the correspondent configuration null-space: $q_{in} \in N(x_d)$). In addition to the above stated, what is also considered a selection condition for the initial configuration q_{in} is the limitation of joint motions physically possible to execute on the Yaskawa SIA10F robot arm, which is used in the physical experiment, by reducing it to the previously defined minimal configuration. Moreover, link lengths of the robot arm mechanism presented in Figure 4 have been adopted to be identical to the Yaskawa SIA 10 F robot arm, that is: l1 = 0.36 m, l2 = 0.36 m, l3 = 0.275 m. In this manner, results of the simulation and the physical verification become comparable.

For the purposes of identification of the achieved task-space TCP stiffness, in the course of executing the previously defined task, robot TCP was excited by the external force F of constant magnitude and in two variants, Exc.#1 and Exc.#2, which are mutually orthogonal (Table I).

3.1 Simulation experiment

The simulation experiment was conducted by applying the Euler method of numerical integration:

$$q(t_i) = q(t_{i-1}) + \delta q(t_i) \tag{14}$$

where ti is the time instance, with adopted quantum of time $\delta t = (t_i - t_{i-1})$ and total simulation interval $i^{max} = k$, while $\delta q(t_i)$ is the total displacement of joint coordinates in the current iteration. The algorithm of the procedure for the calculation of the displacement of joint coordinates according to the set number of iterations (k), reads:

Algorithm: Primary and Secondary Tasks Fusion

input: x_d, K_{xd}, q_{in}, k, δx, δq_{Nmax} (*Table I*)		
output: q_{halt}, K_{x_halt}	Equation	
$K_q(q, K_{xd})$	(3)	Objective function
$u(K_q) \to \delta qc = \nabla(u)$	(9)	
$q_1 = q_{in}$		
for $i=1;\ i<k;\ i=i+1$		
$J(q_i) \to J^+(q_i)$	(7)	
$\delta q_{Pi} = J^+(q_i)\,\delta x = 0$		Primary Task
$\delta qc(q_i) \to \delta q_{Ni} = P^c_{IC}(q_i)$	(12)	Secondary Task
if $\|\delta q_{Ni}\| \le \delta q_{Nmax}$		
then $\delta q_{Ni} = P^c_{IC}$	(13)	Null-Space Stiffness Controller
else $\delta q_{Ni} = (\delta q_{Ni} / \|\delta q_{Ni}\|)\delta q_{Nmax}$		
end if		
$\delta q_i = \delta q_{Pi} + \delta q_{Ni}$	(6)	Tasks Fusion
$q_i = q_{i-1} + \delta q_i$	(14)	
$K_x(q_i)$.	(8)	
end for		
$q_{halt} = q_k$, $K_{x\_halt} = K_x(q_k)$.		

The algorithm generates the homogenous component of the robot arm displacement governed by the secondary task requirements, which modify the initial configuration q_{in} by motion in the configuration null-space, that is, with no effect on the TCP position.

Table I Specification of the two cases of the primary and secondary task used in the experimental verification of the synthesized projector (12)

Parameters of the primary and secondary task	CASE #1		CASE #2	
Primary task $x_d = \{x_{1d}, x_{2d}\}^T$ = const (m)	[0.734, −0.090]		[0.834, −0.190]	
Primary task commanded displacement vector $\delta x = \{\delta x_1, \delta x_2\}^T$ (mm)	[0, 0]		[0, 0]	
Initial Configuration $q_{in} = \{q_{1in}, q_{2in}, q_{3in}\}^T$(rad)	[0.60, −1.70, 1.20]		[0.455, −1.258, 0.472]	
Secondary task hard limit δq_{Nmax} (rad)	0.01		0.01	
Desired shape of task-space TCP stiffness matrix K_{xd} (N/mm)	diag(100,100)		diag(100,100)	
TCP excitation force $F=\{F_{x1}, F_{x2}\}^T$= const (N)	Exc. #1	Exc. #2	Exc. #1	Exc. #2
	[74, 0]	[0, 74]	[74, 0]	[0, 74]

Jacobian matrix $\mathcal{J}(q) \in R^{2\times 3}$ reads:

$$\mathcal{J}11(q) = -\frac{11}{40}sin(q_{123}) - \frac{9}{25}sin(q_{12}) - \frac{9}{25}sin(q_1) \quad (15a)$$

$$\mathcal{J}12(q) = -\frac{11}{40}sin(q_{123}) - \frac{9}{25}sin(q_{12}) \quad (15b)$$

$$\mathcal{J}13(q) = -\frac{11}{40}sin(q_{123}) \quad (15c)$$

$$\mathcal{J}21(q) = \frac{11}{40}cos(q_{123}) + \frac{9}{25}cos(q_{12}) + \frac{9}{25}cos(q_1) \quad (15d)$$

$$\mathcal{J}22(q) = \frac{11}{40}cos(q_{123}) + \frac{9}{25}cos(q_{12}) \quad (15e)$$

$$\mathcal{J}23(q) = \frac{11}{40}cos(q_{123}) \quad (15f)$$

where the following designations were used: $q_1+q_2=q_{12}$ i $q_1+q_2+q_3=q_{123}$, with previously entered link lengths.

3.2 Physical experiment

The experimental platform for the physical verification of the simulation model of isotropic compliance complementary projector consists of the following modules:

- industrial robot Yaskawa SIA10F: redundant anthropomorphic arm, 7 DoF, 1.203 m vertical reach, 0.720 m horizontal reach, payload 10 kg;
- open-architecture robot control system composed of: a) robot controller FS100 (1ms servo loop) running VxWorks RTOS (Real Time Operating System) upgraded with b) real-time open-architecture control and monitoring system Yaskawa MotoPlus SDK (Software Development Kit), integrated into PC based hardware, and equipped with extensive communication interface supported by API (Application Program Interface) access to data transmission, i.e. multi-tasking communication and full socket-based Ethernet network control, and, based on that, control of all robot functions in real-time;
- module for measuring robot arm TCP displacement (laser measurement sensor Omron ZX-LT010 mounted on precise multiaxis stage);
- module for the acquisition of the robot arm TCP displacement.
- module for generating and directing excitation force to the robot TCP;

Application of the open-architecture control concept allowed physical implementation of the following functions:

- reducing 7 DoF of the Yaskawa SIA10F robot arm to 3 DoF, the physical equivalent of the minimal planar redundant configuration (presented in Figure 4), through software passivation of joints 2, 3, 5, 7 (completely inactive during the experiment – blocked actuators), while joints 1, 4, 6 are active;
- practical implementation of the synthesized isotropic compliance projector (12) in real time, that is, calculation and execution of the homogenous motion component $\delta q_N = P^c_{IC}(q)$ in configuration null-space; and
- real-time monitoring of coordinates and actuation torques of all active joints by using Ethernet serial communication.

Such experimental platform allows motion control of the Yaskawa SIA10F robot arm, which simultaneously performs primary and secondary tasks. The architecture of the robot experimental platform is presented in Figure 5, and a photo of the actual system is presented in Figure 6.

The system for generating excitation of the robot TCP by static force is based on the application of a weight and a suitable mechanical mechanism for precise direction of the excitation

Figure 5 Experimental system architecture

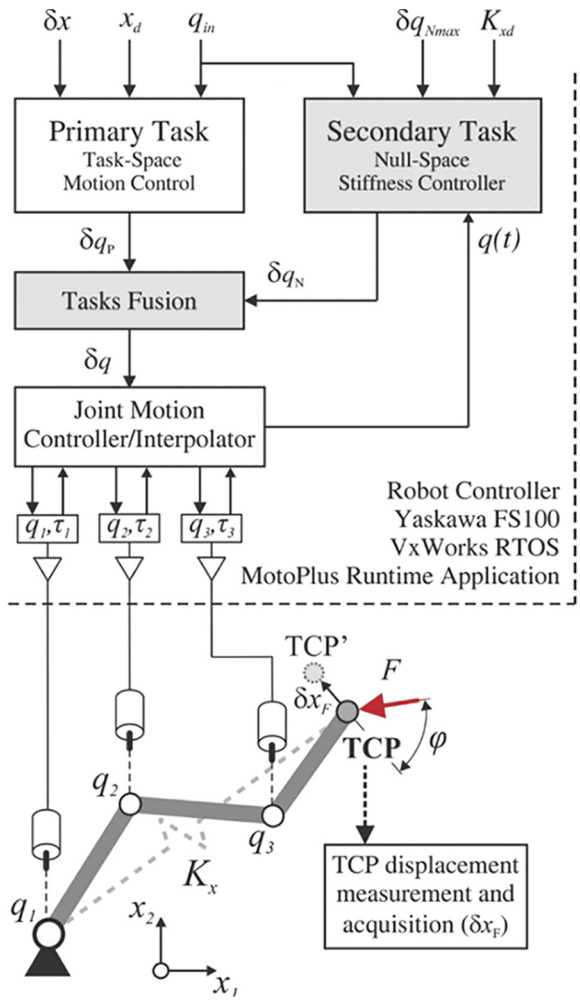

Notes: Task-space motion control and null-space stiffness controller – primary and secondary task implemented by MotoPlus SDK – open-architecture control; real-time robot controller FS100 based on VxWorks operating system, including MotoPlus Runtime Application for primary and secondary tasks fusion and execution; SIA10F robot arm in planar kinematically redundant 3 DoF configuration – physical equivalent of the minimal configuration simulation model

Figure 6 Experimental platform for physical verification of the proposed concept of control of the elastomechanical properties of the Yaskawa SIA 10F robot arm joint mechanism, based on isotropic compliance complementary projector (12)

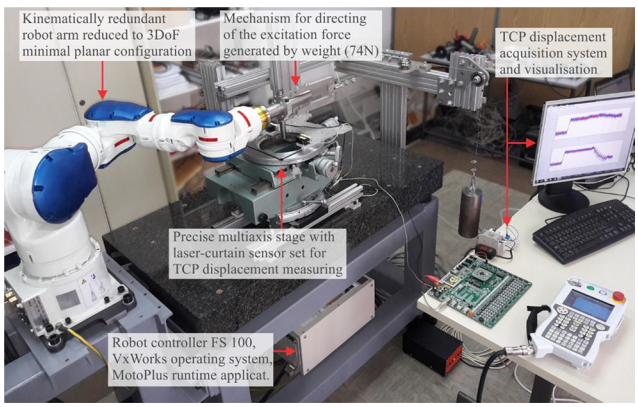

force and its routing to the robot TCP (Figure 7). The nominal value of the static excitation intensity is F = 74N.

The system for measuring both components of the robot TCP planar displacement δ_{xF} is based on high-resolution non-contact sensors Omron ZX-LT010. This sensor works on the principle of optical curtain shading and is composed of plane-parallel optical emitter and receiver, which generate analog output signal in a 10-mm working range, with digital resolution of 0.003 mm provided by 12-bit analog-to-digital conversion used in experimental measurements.

Robot TCP coincides with the central axis of the precise grinded pivoting pin, 20 mm in radius. Precise multiaxis stage (two-axis translation and single-axis rotation) as part of the system for measuring 2D displacement of robot TCP is used for precise rotational and translatory positioning of the optical sensor in robot task-space, according to the nominal position of the TCP $x_d \in R^2$. A graphic representation of the measuring principle of robot TCP displacement and a corresponding photo are presented in Figure 8.

3.3 Results and discussion

Results of the simulation experiment with the parameters listed in Table I (CASE#1 and CASE#2) and for the number of iterations k = 200 are presented in Figure 9. The initial configuration is marked blue, and the terminal, that is, halting configuration, q_{halt}, for iteration k = 200, is marked red. For the sake of clarity, the robot arm mechanism configurations

Figure 7 System for generating excitation of the robot TCP by static force of continuous intensity in the desired direction in two configurations (CAD model): Exc.#1 (left) and Exc.#2 (right)

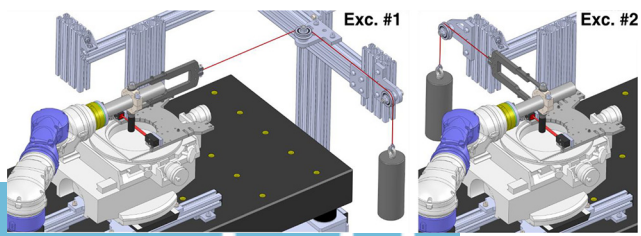

Figure 8 System for measuring robot TCP displacement vector

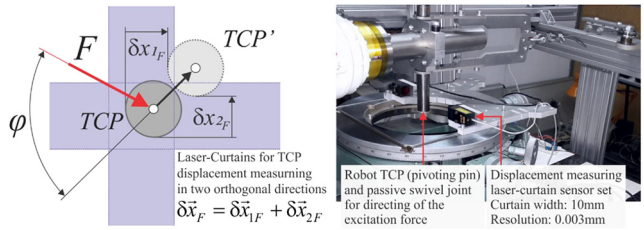

Notes: Displacement measuring principle based on laser curtain in two mutually orthogonal directions by applying optical sensor Omron ZX-LT010 (left) and a photo of physically implemented measurement system (right)

presented show every tenth iteration. Robot arm motion from qin to q_{halt} was produced solely under the effect of the isotropic compliance projector (12). TCP zero motion is obvious during the entire simulation experiment, which clearly indicates that the execution of the secondary task has not affected the execution of the primary task and that robot arm motion took place exclusively within the configuration null-space. Joint displacement vector δq_i is presented in Figure 9c for CASE#1 and CASE#2 repsectively. Motion is smooth and it does not exceed the limit value δq_{Nmax} defined in Table I, according to equation (13) – hard limit. It is notable that the complete execution of the secondary task is achieved before the simulation interval ends (k = 200). Robot arm enters the steady-state configuration, q_{steady}, in iteration k = 172 for CASE#1 and k = 161 for CASE#2. This configuration is presented by a black marker in Figures 9c and 9d and determined by the criterion of zero joint displacement vector $\delta q_{i+1} = \delta q_i = 0$.

Figure 10 presents the achieved values of the elements of the task-space TCP stiffness matrix K_x during the simulation experiment presented in Figure 9. A circular marker is used in CASE#1, and a square marker in CASE#2. It can be observed that, during the transition from the initial configuration, q_{in}, to the terminal, q_{halt}, the elements of matrix K_x change their values smoothly and without discontinuity, whereby the off-diagonal element ($k_{x12} = k_{x21}$) has a clearly expressed convergence to zero value, effectively following the objective function (9). The value of the objective function (9) and its derivative is presented in Figures 10b and 10c, respectively.

By careful observation of the value of the off-diagonal element $k_{x12} = k_{x21}$ it can be noticed that the horizontal coordinate axis is crossed at one point, that is, the value equals zero, which means that the initial off-diagonal stiffness matrix K_{x_in} translates to a diagonal shape. Specifically, it happens in iteration i = 100 for CASE#1 and iteration i = 132 for CASE#2. Continued simulation process results in the off-diagonal element having non-zero value once again. This fact indicates that the synthesized projector (12) is not optimal, that is, that the objective function (9) is not optimal and that there is a better solution, which is outside our reach at the moment. At the same time, the obtained simulation results indicate that the synthesized projector (12) is effective and that it translates the robot configuration in a stable manner from the initial position qin with highly anisotropic TCP stiffness K_{x_in} = (K_{x11} = 404.93, K_{x12} =

Figure 9 Null-space motion of the minimal configuration robot arm mechanism from initial, q_{in}, to terminal, q_{halt}, configuration under the effect of the isotropic compliance complementary projector (12), CASE#1 (left) and CASE#2 (right)

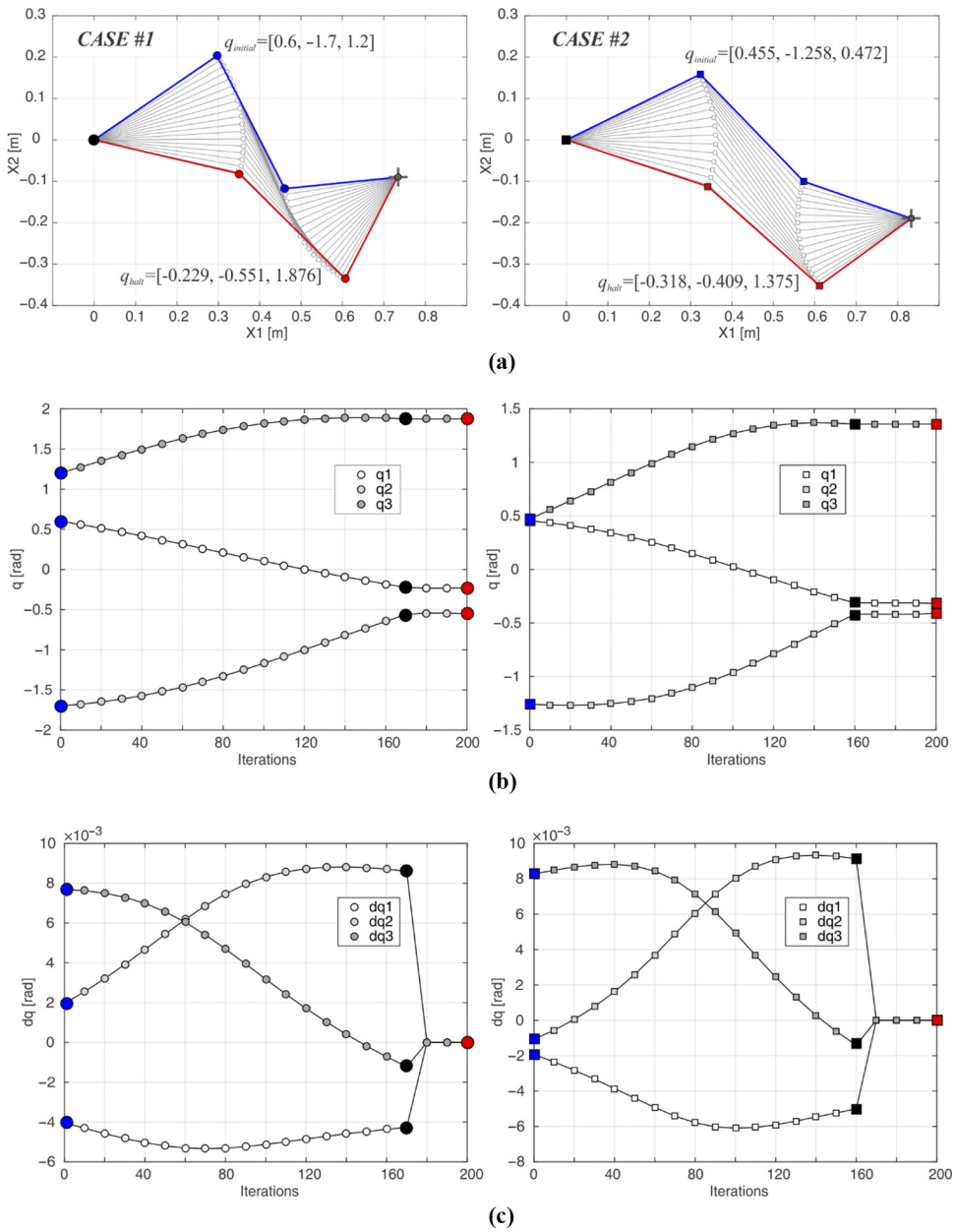

Notes: (a) Motion in x_1x_2 task-space; (b) joint coordinates vector; (c) joint displacement vector

-113.73; $K_{x21} = -113.73$, $K_{x22} = 71.91$) for CASE#1 and $K_{x\_in} = (K_{x11} = 790.18$, $K_{x12} = -325.74$; K_{x21}=-325.74, $K_{x22} = 169.37$) for CASE#2, to the steady-state configuration q_{steady}, in which the achieved TCP stiffness is sufficiently close to quasi-isotropic shape, that is $K_{x\_steady} = (K_{x11} = 106.4$, $K_{x12} = 21.42$; $K_{x21} = 21.42$, $K_{x22} = 45.71$) for CASE#1 and $K_{x\_steady} = (K_{x11} = 187.27$, $K_{x12} = 15.60$; $K_{x21} = 15.60$, $K_{x22} = 28.193$) for CASE#2. The previously mentioned diagonal shape with purely quasi-isotropic TCP stiffness determines the optimal configuration. The optimal configuration is marked green in graphs in Figure 10, where $Kx\_100 = K_{x\_opt}$ = diag ($K_{x11} = 130.7$, $K_{x22} = 44.7$) for CASE#1 and $K_{x\_132} = K_{x\_opt}$ = diag($K_{x11} = 179.6$, $K_{x22} = 31.5$) for CASE#2. The listed values of the stiffness matrix elements are expressed in N/mm.

In accordance with the general formal framework stated in subchapter 2.2, the kinetostatic properties in the task-space are completely determined by eigenvalues and eigenvectors of the TCP stiffness matrix K_x, equation (4). In the case considered,

Figure 10 Completing of the secondary task under the effect of complementary projector (12), as a consequence of motion in the configuration null-space presented in Figure 9

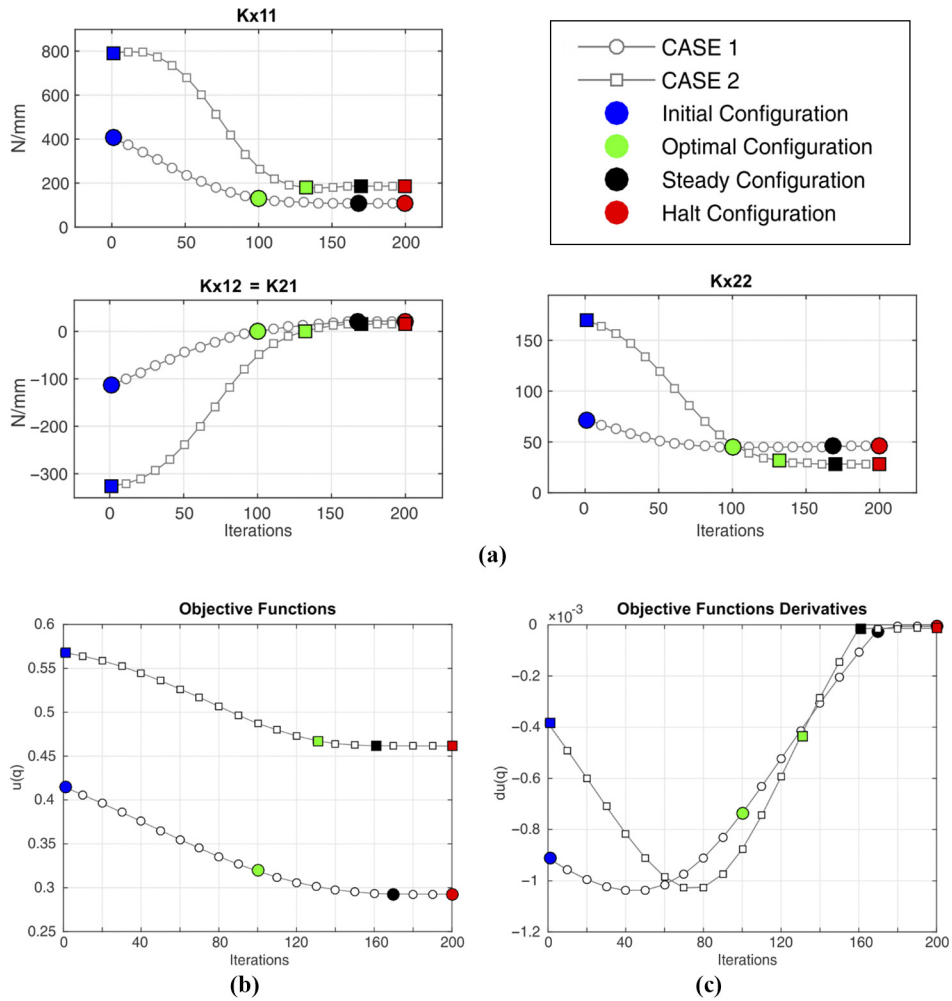

Notes: (a) Change of value of the task-space TCP stiffness matrix Kx (top); (b) objective functions (bottom left); (c) objective function derivative (bottom right)

there are two eigenvalues, λ_{x1} and λ_{x2}, with related eigenvectors, ν_1 and ν_2, so the following can be written (Lay, 2005):

$$K_x(q)v_i = \lambda_{xi}v_i \xrightarrow{m=2} \begin{cases} \begin{bmatrix} k_{x11}(q) & k_{x12}(q) \\ k_{x21}(q) & k_{x22}(q) \end{bmatrix} \begin{bmatrix} v_{11} \\ v_{12} \end{bmatrix} = \lambda_{x1} \begin{bmatrix} v_{11} \\ v_{12} \end{bmatrix} \\ \begin{bmatrix} k_{x11}(q) & k_{x12}(q) \\ k_{x21}(q) & k_{x22}(q) \end{bmatrix} \begin{bmatrix} v_{21} \\ v_{22} \end{bmatrix} = \lambda_{x2} \begin{bmatrix} v_{21} \\ v_{22} \end{bmatrix} \end{cases} \tag{16}$$

which yields the following ellipse equation (Lockwood, 1961), expressed through eigenvalues and eigenvectors of the task-space TCP stiffness matrix K_x:

$$\frac{(x_{1p} \cdot v_{11} + x_{2p} \cdot v_{12})^2}{\lambda_{1x}^2} + \frac{(x_{1p} \cdot v_{21} + x_{2p} \cdot v_{22})^2}{\lambda_{2x}^2} = 1 \tag{17}$$

which visualizes the kinetostatic properties of the considered robot mechanism TCP, where x_{1p} and x_{2p} are coordinates of an arbitrary point on the ellipse. Rotation of the ellipse principal axes relative to the coordinate system of the task-space, angle θ (Figure 3a), can be calculated from eigenvectors:

$$\theta = \arccos\left(\frac{\overrightarrow{v_1} \cdot \overrightarrow{x_{1u}}}{||\overrightarrow{v_1}|| \, ||\overrightarrow{x_{1u}}||}\right) \tag{18}$$

where ν_1 is the eigenvector of the major ellipse principal axis and x_{1u} is a unit vector of the task-space coordinate axis x_1.

From the generated series of matrix K_x values, represented graphically in Figure 10 and based on expression (17) and (18), a change in the kinetostatic properties of the robot mechanism can be visualized by its motion in the configuration null-space under the effect of the complementary projector (12), Figure 11. Ellipses presented in Figures 11a and 11b are normalized according to the highest eigenvalue in the complete simulation experiment. It is obvious that the complementary projector (12) has an essential effect on the elastomechanical properties of the robot mechanism TCP, altering the relative relation of the matrix K_x eigenvalues and the orientation of its

Figure 11 Simulation experiment: robot arm motion in the configuration null-space (left), during the execution of the secondary task and the corresponding evolution of the stiffness ellipsis (right), with indicated and marked characteristic configurations

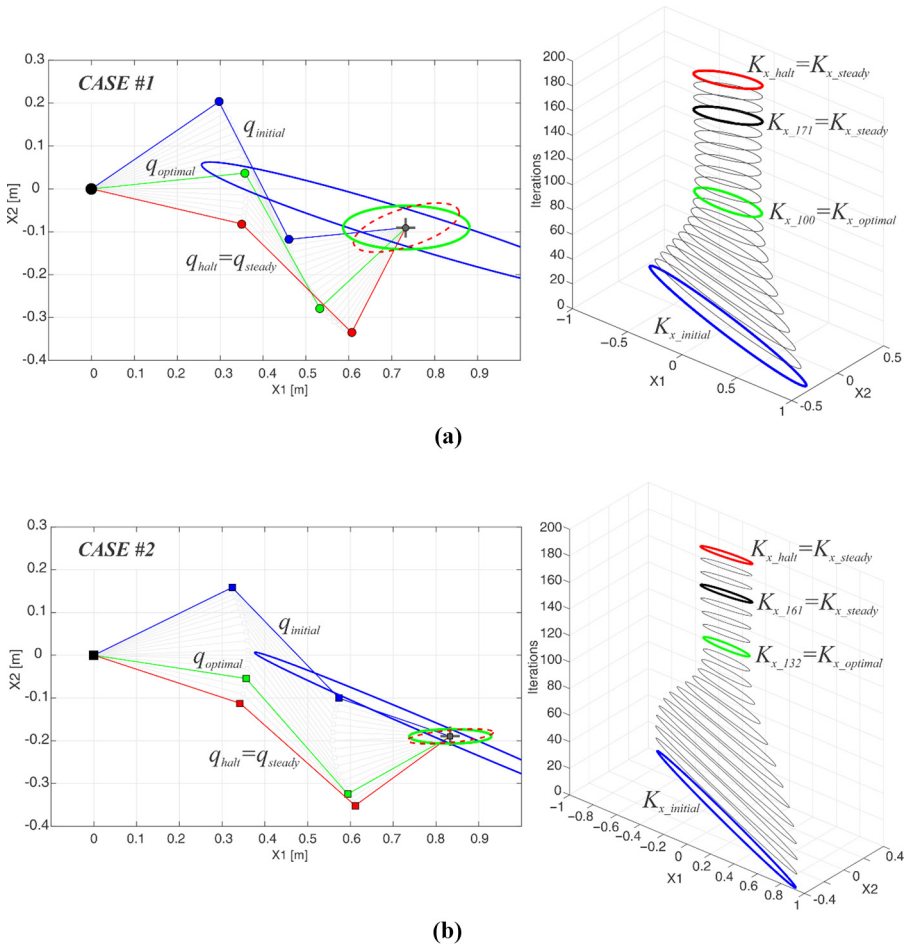

Notes: (a) CASE#1 (top); (b) CASE#2 (bottom)

principal axis in relation to the adopted coordinate system of the task-space.

It is obvious that changes in the stiffness ellipse in both simulation experiments have a very intensive character. The changes refer rather equally to the change in the ellipticity (conditioned by the change of matrix K_x eigenvalues) and the change of the rotation angle of the principal coordinate system in relation to the arbitrarily chosen coordinate system of the task-space. Complementary projector (12) makes a deep impact on the kinetostatic properties of the considered robot arm.

Physical verification was conducted on the experimental robot platform described in section 3.2, by executing both variants of the task (CASE#1 and CASE#2), equivalent in all respects to the previously described simulation experiment. Motion of the SIA 10 F robot arm in the configuration null-space was governed by the physical execution of the complementary projector (12) in real time, using the functionality of the open-architecture robot controller applied to the Yaskawa SIA 10 F experimental robot platform. Identification of the kinetostatic properties during this motion was conducted indirectly, in a discrete measurement series of the robot TCP displacements, δ, as a response to the external excitation by force F_x, which was achieved in accordance with the parameters defined in Table I. To create the conditions for comparing simulation results and the results achieved using the SIA 10 F robot, displacements of the robot TCP in the simulation experiment were calculated by means of applying relation (1). This generated two corresponding time series of the robot TCP displacement of the SIA 10 F robot, δx_{F_rob} and the TCP displacement of the simulation model, δx_{F_sim}.

The signal of the measured robot TCP displacement δx_{F_rob} is very complex, and, unlike the results of the simulation, δx_{F_sim}, produced using an idealized kinematic model, it contains traces of a series of physical phenomena such as: friction, backlash in the actuation system or effects of the discrete nature of the servo-actuator control component, which generates dynamic excitation that spreads as a disturbance throughout the entire robot arm mechanism, all the way to the TCP. Moreover, there should also be no disregard for the effect of the motion control interpolation algorithms of the robot joints, with unknown approximations that

Figure 12 Physical verification of the complementary projector (12), CASE#1 – comparative display of the idealized simulation and physically measured response (displacement) of the robot TCP to the excitation force Exc.#1 and Exc#2

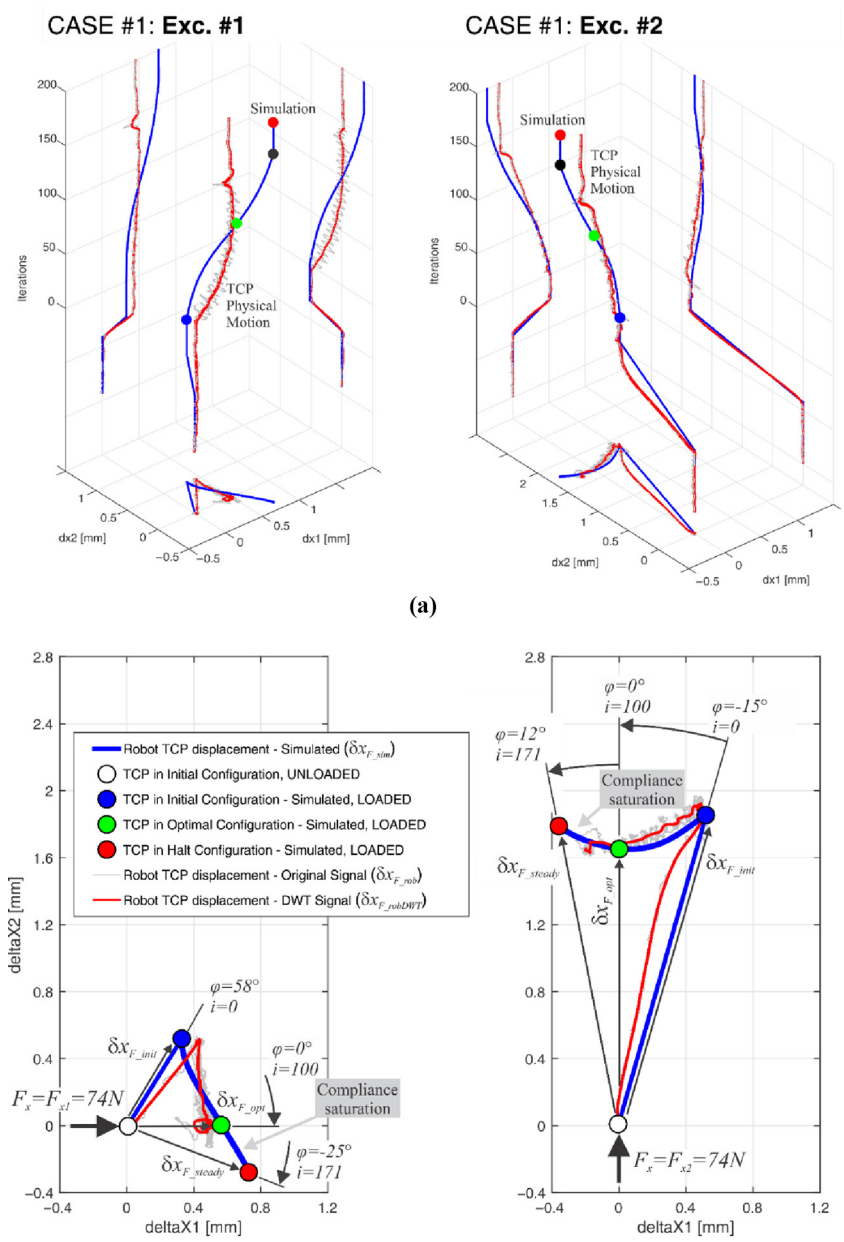

Notes: (a) 3D graphic representation of TCP behavior during the iterative effect of the complementary projector (12); (b) 2D projection on the task-space with designated response vectors in characteristic configurations and correspondent collinearity angles in line with equation (5)

the manufacturer of the Yaskawa SIA10F robot had to build into the robot controller to ensure efficient calculation of the enormously complex Jacobian (the entire robot arm has 7 degrees of freedom). The starting premise of the conducted analysis of the measured robot TCP displacements was that the changes in the kinetostatic properties of the robot arm mechanism, conditioned by the execution of the secondary task, are contained exclusively in the low-frequency components of the measured signal and that they dominantly determine their character. This is why, to identify experimentally the actual effects of the complementary projector (12) on the kinetostatic properties of the SIA 10F robot arm, a multiresolution decomposition of the measured signal was conducted on 12 components using Discrete Wavelet Transformation (DWT) by applying Daubechies wavelet db5. The original signal δx_{F_rob} and its corresponding low-frequency DWT level 10 approximation,

Figure 13 Physical verification of the complementary projector (12), CASE#2 – comparative display of the idealized simulation and physically measured response (displacement) of the robot TCP to the excitation force Exc.#1 and Exc.#2

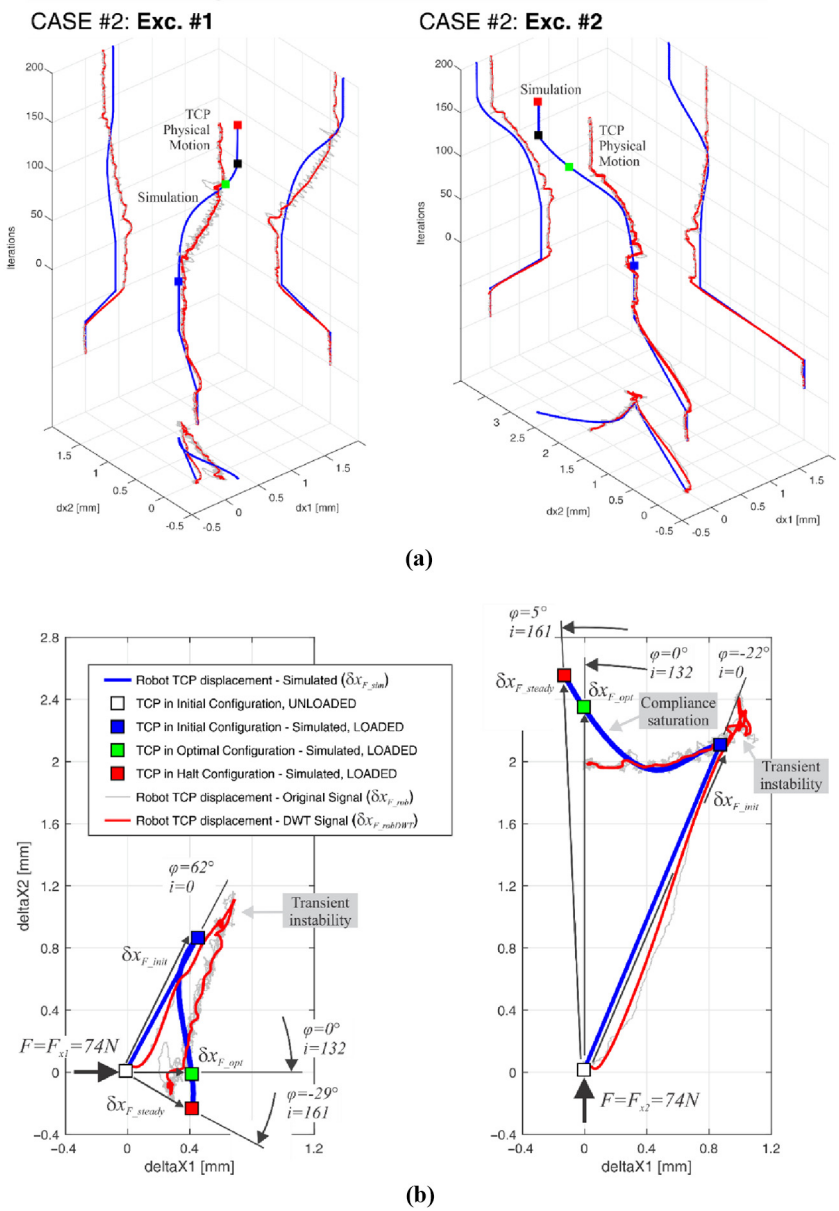

Notes: (a) 3D graphic representation of TCP behavior during the iterative effect of the complementary projector (12); (b) 2D projection on the task-space with designated response vectors in characteristic configurations and correspondent collinearity angles in line with equation (5)

δx_{F_robDWT}, are presented in Figures 12 and 13, along with the equivalent displacement δx_{F_sim}, calculated based on the TCP stiffness matrix, K_x, obtained in the previously described simulation experiments, under the effect of the virtual excitation by external force.

Figure 12a (CASE#1) and Figure 13a (CASE#2) present robot TCP motion with the parameters listed in Table I. Robot TCP motion in both experimental variants, the simulation experiment (blue) and the physical experiment (red), is presented as a function of time, with the quantum of time $\delta t = 0.2$ sec, where time axes of the simulation and the physical experiments have been alienated. The origin of the time axis of the physical experiment was translated to the moment when the motion of the SIA 10 F robot arm was activated. Presentation of the time horizon $t = 0$ is preceded by the sequence of introducing physical excitation (Exc.#1 or Exc.#2), which implied robot TCP displacement determined by the joint-space stiffness matrix $K_q = \text{diag}(k_{11}, k_{22}, k_{33})$ and the initial robot configuration $q_{init} = [q_1, q_2, q_3]T$. Components of the joint-space stiffness matrix K_q have been identified experimentally

as: K_q = diag(49.2, 18.4, 5.5), expressed in (Nm/rad). It is obvious that, contrary to the significant unmodelled content, there is a clear correlation between the robot TCP motion obtained in the simulation experiment and the one obtained in its corresponding physical experiment. This is indicative of two very important facts:

1 physical stiffness of the SIA 10F robot arm TCP is dominantly determined by its configuration, regardless of the presence of a number of disturbing factors; and
2 the developed experimental platform, which is essentially based on the commercially available robot Yaskawa SIA 10F, can, with an adequate upgrade of the control system, physically perform the complementary projector (12) with a high degree of correlation with the idealized simulation model.

Projection of the 3d representation of the TCP trajectory on the horizontal plane eliminated time as a parameter, which allowed objective insight into the results of the implementation of the complementary projector (12) in the physical system. An obviously high degree of correlation of the simulation and the physical behavior indicates that the set concept is practically applicable and that this approach can be used to control robot TCP stiffness effectively by motion within the configuration null-space and in accordance with the adopted objective function, which that motion is determined by. Graphs in Figures 12b and 13b confirm the previously stated claims. Their further analysis offers concrete quantitative argumentation. Projections on the profile/lateral planes of the 3d graph presented in Figures 12 and 13 allow simple quantification of the deviation of the robot SIA 10 F TCP physical motion in relation to the idealized TCP motion obtained in the simulation. The maximum deviation δx_{F_max}=max(norm (δx_{F_robDWT}, δx_{F_sim})) for both cases considered is: CASE#1: Exc.#1-δx_{F_max} = 0.406 mm, Exc.#2-δx_{F_max} = 0.173 mm, CASE#2: Exc.#1-δx_{F_max} = 0.36 mm, Exc.#2-δx_{F_max} = 0.788mm, while the mean-square deviation δx_{F_RMS}=mean(norm(δx_{F_rob}, δx_{F_sim})) is: CASE#1: Exc.#1-δx_{F_RMS} = 0.218mm, Exc.#2-δx_{F_RMS} = 0.1 mm, CASE#2: Exc.#1-δx_{F_RMS} = 0.149mm, Exc.#2-δx_{F_RMS} = 0.439 mm. To understand these values fully, they should be compared to the robot accuracy, which, according to the specifications of the manufacturer in the case of robot SIA 10 F and robot controller FS100, equals ±0.1 mm.

The stated deviations, especially the extreme ones, which as a rule appear in the final phase of the secondary task execution, can potentially be explained by the phenomenon of saturation, that is, by the physical limitations of the actuation mechanism (including the related servo-controller) driving the joints of the SIA 10 F robot arm (another essential difference between the physical robot arm and its conditionally equivalent idealized abstract simulation model). Saturation means that maximum possible joint displacement of one or more joints has been achieved in a certain configuration of the robot arm under the effect of excitation force F_x, and that, as a consequence of that occurrence, relative TCP displacement achieved in the simulation experiment has not been reached physically.

Figures 12b and 13b present orthogonal views on the non-parametric plain from Figures 12a and 13a, respectively, with indicated TCP displacement vectors δx_{F_init}, δx_{F_opt}, and δx_{F_steady}, which are correspondent to configurations q_{init}, q_{opt}, and q_{steady}, presented in Figure 11a and 11b. For the sake of full clarity, it is necessary to emphasize that the set initial position of the robot TCP, x_d = {x_{1d}, x_{2d}}, was moved to the origin of the task-space coordinate system to directly read the values of the relative TCP displacement, $\delta x_F(t)$, during the physical and the simulation experiment. It is evident that the kinetostatic properties of the robot arm TCP in the initial configuration are such that the displacement vector δx_{F_init} is not collinear with the vector of the excitation force F_x (Exc.#1 and Exc.#2 in Table I). By applying relation (5), the following is calculated (simulation and physical experiment): CASE#1, Exc.#1−φ_{init} = 58° (physically: 50°) and for Exc.#2−φ_{init} = −15° (−15°); while for CASE#2 the following applies: Exc. #1−φ_{init} = 62° (−59°) and Exc.#2 − φ_{init} = −24° (−24°). These values are consistent with the TCP stiffness matrix K_x defined by relation (8), that is, by the results obtained in the simulation experiments. For the configuration designated q_{opt}, the achieved TCP displacement is ideally aligned with the vector of excitation F_x, which leads to φ_{opt} = 0°. However, as indicated by the results of the simulations and physical experiments, the complementary projector (12), which governs arm motion during the execution of the secondary task, does not stop robot arm motion in q_{opt}; instead, it continues to q_{steady}. By reaching q_{steady} configuration, the robot arm enters the state of inaction, which is maintained until halting of the secondary task control sequence, that is, q_{halt} = q_{steady} applies. As a result, achieved collinearity in configuration q_{opt} is lost in q_{steady}, thus CASE#1, Exc.#1-φ_{steady} = φ_{halt}=−25° (physically: ∼0° - consequence of saturation) and CASE#1, Exc. #2−φ_{steady} = φ_{halt} = 12° (6° − consequence of saturation); while for CASE#2, Exc.#1-φ_{steady} = φ_{halt} = −29° (-20°) and for CASE#2, Exc.#2-φ_{steady} = φ_{halt} = 5° (∼0° - consequence of saturation). Such behavior poses the question of the actual effectiveness of the proposed complementary projector, i.e. whether the choice of the objective function (9), which it is based on, is optimal.

By careful observation of the corresponding stiffness ellipses, Figure 11, it can be noted that the principal axes of the stiffness ellipse are aligned with the axes of the adopted task-space coordinate system in all configurations q_{opt}, identified for CASE#1 and CASE#2. Therefore, the evident collinearity is not a consequence of the actual isotropy of configuration q_{opt}.

The state closest to kinetostatic isotropy is achieved in all experiments in configuration q_{steady}, which leads to the conclusion that the complementary projector (12) is convergent and stable in its local or, potentially, global minimum. In this paper we do not offer proof that the achieved minimum is also global, that is, that robot arm motion within the configuration null-space, governed by the complementary projector (12), resulted in its transition from the arbitrary initial configuration to the best possible configuration from the aspect of kinetostatic isotropy, i.e. that q_{halt} = q_{steady} = q_{opt}. It can be claimed with certainty that, without producing an effect on the primary task, null-space motion governed by the objective function (9) of the complementary projector (12) causes convergent transition of the arbitrary initial configuration q_{init}

of the kinematically redundant robot with monoarticular actuation system in all joints and with constant joint space stiffness matrix, i.e. K_q = const, to the asymptotically stable configuration q_{steady}, for which the following is always true:

- ellipse of the TCP stiffness matrix K_{x_steady} has lower ellipticity than the ellipse of the TCP stiffness matrix K_{x_init}; and
- the Euclidian norm of off-diagonal elements of congruence transformation (3), for configuration q_{steady}, has lower value in relation to configuration q_{init}.

4. Conclusion and further research

In this paper, we presented the results of theoretical and experimental research into the impedance control of kinematically redundant robot arm in the process of robotic part mating of high geometrical precision assemblies (for example, precise motor assemblies in the automotive industry). With Whitney's theory of quasistatic part mating and its practical implementation on the RCC unit as the starting point, along with the general concept of simultaneous execution of two or more tasks on a kinematically redundant robot arm mechanism, a complementary projector was synthesized which makes it possible to control null-space stiffness and achieve robot TCP stiffness properties equivalent or sufficiently similar to the isotropic properties of the RCC unit. As opposed to the RCC unit, which is a passive and, consequently, inflexible mechanical structure, using this approach makes robot TCP stiffness a process variable, which can be controlled in real time.

Complementary projector for null-space stiffness control is synthesized based on the objective function, which minimizes the Euclidian norm of off-diagonal elements of the joint-space stiffness matrix, K_q, whereby the joint-space stiffness matrix K_q is determined by the congruent transformation of the desired task-space TCP stiffness, K_{xd}, that is $K_q = f(q, K_{xd})$, in the configuration subspace defined by the requirements of the primary task execution, that is, by the robot TCP position control. Minimization, or complete elimination of the off-diagonal elements of the joint-space stiffness matrix K_q is of essential importance in application to robot arms with monoarticulated joints because this type of actuation (*de facto* the only technically achievable solution as long as the biological systems remain outside our reach!) cannot physically generate off-diagonal elements which do not equal zero, nor can it, therefore, produce the desired matrix of task-space TCP stiffness.

Behavior of the synthesized complementary projector (12) was first verified in simulation, and then in physical experiments, by its implementation on the commercially available redundant anthropomorphic robot Yaskawa SIA10F, equipped with an open-architecture control system and a system for generating mechanical excitation and measuring response, i.e. robot TCP displacement. Two series of simulation and physical experiments have been conducted with planar, kinematically redundant robot arm (minimal redundant configuration with 2d task-space TCP stiffness matrix K_x). Parameters of the simulation model were adopted to be identical to the parameters of the physical robot arm obtained by reducing the redundant anthropomorphic robot Yaskawa SIA 10 F (which has 7 degrees of freedom) to the planar redundant configuration with 3 degrees of freedom. In addition, the conducted simulation and physical experiments were mutually equivalent to allow a comparison of the real-life physical system behavior to the idealized simulation model. The idealized simulation model was used as a reference model in the conducted experimental research.

Simulation experiments conclusively indicate that the complementary projector (12) intensely affects the kinetostatic properties of the robot arm, whereby the off-diagonal elements of the joint-space stiffness matrix converge stably to the value minimizing the objective function (9). At the same time, in robot task-space, elements of the task-space TCP stiffness matrix converge stably to the values defined by the desired stiffness matrix K_{xd}, to the point which is physically achievable. Graphic visualization of the evolution of robot arm kinetostatic properties from initial (determined by the arbitrarily selected initial robot arm configuration) to final, was achieved by virtue of the stiffness ellipse. The stiffness ellipse is analytically determined by the eigenvalues and eigenvectors of the task-space TCP stiffness matrix, K_x. All simulation experiments have shown that kinetostatic properties of the robot arm converge stably to the desired state of mechanical isotropy, that is, that the initial stiffness ellipse converges stably to a circle when eigenvalues reach relative proximity. Maximum degree of reduction in the ellipticity of the stiffness ellipse, that is, maximum possible approximation of the robot arm kinetostatic properties to the state of isotropy is eventually determined by the stiffness or robot joints.

Physical experiments have demonstrated that application of the complementary projector (12) on the commercially available robot arm Yaskawa SIA 10 F is practically possible to implement, that is, that, in the course of executing the secondary task with real physical systems, the complementary projector (12) achieves a change in the kinetostatic properties, which:

- is measurable; and
- stably converges to a state which is more favorable from the aspect of requirements of the robotic assembly process.

High-resolution measurements obtained by using laser sensors with optical curtain have shown that the process of evolution of kinetostatic properties is significantly affected by unmodelled phenomena, especially friction and task execution actions of the FS100 robot control system, but it is clear that the dominant behavior of the physical system corresponds to the behavior obtained in simulation experiments with an idealized equivalent model of the robot arm. Removing high-frequency components using multiresolution phase decomposition of the original sensor signal of robot TCP displacement in two coordinate directions of the robot task-space, achieved by virtue of discrete wavelet transformation (DWT) and Daubechies wavelet db5, resulted in effective extraction of the component produced by the complementary projector (12). All experiments demonstrated a high degree of correlation between the physical and simulation models, which leads to the conclusion that the proposed model of robot arm compliance control is generally sustainable and that it represents a good foundation for further research aimed at its enhancement, and, eventually, its practical implementation as an alternative to the

conventional RCC unit, but with flexibility properties which the RCC unit does not possess. Irrespective of the fact that the experiments were conducted in the planar task-space with 2DoF using anthropomorphic robot arm reduced to the minimal redundant quasi 3DoF planar configuration, all findings and previously derived conclusions, without limitation, apply to the case of complete 6 D task-space. This attitude is valid with a limitation that neither relation (2), nor, consequently, projector (12), encompass the gravitation member.

The final solution to the problem considered is probably a compromise or a hybrid solution, which will be based on the simultaneous use of a type of an RCC unit as a passive physical element, which reduces TCP stiffness of the kinematically redundant robot arm, and a system based on the complementary projector, which, by stiffness control in the configuration null-space, allows the required flexibility of the entire robotic system. The experimental research conducted demonstrated that minimal redundancy mechanisms, order $r = n - m = 1$, do not have the sufficient capacity to control eigenvalues of the robot arm TCP task-space stiffness matrix K_x. The solution to this problem requires combined approach, that is, control of null-space stiffness and application of variable stiffness actuators (VSA).

Additionally, certain shortcomings and limitations have been noticed, the cause of which is primarily the imperfection of the robot arm actuation mechanism (non-linearity of backlash type and friction), and limitations in the sense of saturation and achievable joint compliance allowed by the actuation mechanism and the robot arm control system. In this regard, a number of questions remain open as concerns singularity avoidance, dynamical consistency, as well as the required dimensionality of configuration null-space, that is, kinematic redundancy ($r = n - m$) and its implications for the secondary task(s) performance.

References

Ajoudani, A., Tsagarakis, N. and Bicchi, A. (2015), "On the role of robot configuration in Cartesian stiffness control", in *IEEE International Conference on Robotics and Automation (ICRA), 26-30 May*, *IEEE*, *Seattle, WA*, pp. 1010-1016.

Albu-Schaffer, A., Fischer, M., Schreiber, G., Schoeppe, E. and Hirzinger, G. (2004), "Soft robotics: what Cartesian stiffness can we obtain with passively compliant, uncoupled joints?", *IEEE/RSJ International Conference on Intelligent Robots and Systems, 28 Sept.-2 Oct*, *IEEE*, *Sendai*, pp. 3295-3301.

Baerlocher, P. and Boulic, R. (2004), "An inverse kinematic architecture enforcing an arbitrary number of strict priority levels", *The Visual Computer*, Vol. 20 No. 6, pp. 402-417.

Baillieul, J., Hollerbach, J. and Brockett, R. (1984), "Programming and control of kinematically redundant manipulators", *23-rd IEEE Conference on Decision and Control, 12-14 Dec*, *IEEE*, *Las Vegas, NV*, pp. 768-774.

Chen, H., Wang, J., Zhang, G., Fuhlbrigge, T. and Kock, S. (2009), "High-precision assembly automation based on robot compliance", *The International Journal of Advanced Manufacturing Technology*, Vol. 45 Nos 9/10, pp. 999-1006.

Ciblak, N. and Lipkin, H. (1996), "Remote center of compliance reconsidered", *Proceedings of The ASME Design Engineering Technical Conference and Computers in Engineering, 18-22 Aug*, *ASME*, *Irvine, CA*, pp. 1-10.

Craig, J. (2005), *Introduction to Robotics*, Pearson Education International, New York, NY.

De Fazio, T., Seltzer, D. and Whitney, D. (1984), "The instrumented remote center compliance", *Industrial Robot*, Vol. 11 No. 4, pp. 238-242.

Dedong, G., Yong, L. and Haojun, Z. (2012), "Needle steering for robot-assisted insertion into soft tissue: a survey", *Chinese Journal of Mechanical Engineering*, Vol. 25 No. 4, pp. 629-638.

Dietrich, A., Albu-Schaffer, A. and Hirzinger, G. (2012), "On continuous null space projections for torque-based, hierarchical, multi-objective manipulation", in *IEEE International Conference on Robotics and Automation, 14-18 May*, *Saint Paul, MN*, *IEEE*, pp. 2978-2985.

Dietrich, A., Ott, C. and Albu-Schaffer, A. (2015), "An overview of null space projections for redundant, torque-controlled robots", *The International Journal of Robotics Research*, Vol. 34 No. 11, pp. 1385-1400.

Dietrich, A., Wimbock, T. and Albu-Schaffer, A. (2011), "Dynamic whole-body mobile manipulation with a torque controlled humanoid robot via impedance control laws", *IEEE/RSJ International Conference on Intelligent Robots and Systems (IROS), 25-30 Sep*, *IEEE*, *San Francisco, CA*, pp. 3199-3206.

Flacco, F., De Luca, A. and Khatib, O. (2015), "Control of redundant robots under hard joint constraints: saturation in the null space", *IEEE Transactions on Robotics*, Vol. 31 No. 3, pp. 637-654.

Hogan, N. (1985), "Impedance control: an approach to manipulation, part I-theory, part II-implementation, part III-application", *Journal of Dynamic Systems, Measurement, and Control*, Vol. 107 No. 1, pp. 1-24.

Huang, T., Li, C., Wang, Z., Liu, Y. and Chen, G. (2016), "A flexible system of complex surface polishing based on the analysis of the contact force and path research", *IEEE International Workshop on Advanced Robotics and its Social Impacts (ARSO), July 8-10*, *IEEE*, *Shanghai*, pp. 289-293.

Jovane, F., Koren, Y. and Boer, C. (2003), "Present and future of flexible automation-towards new paradigms", *CIRP Annals - Manufacturing Technology*, Vol. 52 No. 2, pp. 543-560.

Karami, A., Sadeghian, H., Keshmiri, M. and Oriolo, G. (2018), "Hierarchical tracking task control in redundant manipulators with compliance control in the null-space", *Mechatronics*, Vol. 55, pp. 171-179.

Kazerooni, H. (1988), "Robotic deburing of two-dimensional parts with unknown geometry", *Journal of Manufacturing Systems*, Vol. 7 No. 4, pp. 329-338.

Khatib, O. (1987), "A unified approach for motion and force control of robot manipulators: the operational space formulation", *IEEE Journal on Robotics and Automation*, Vol. 3 No. 1, pp. 43-53.

Khatib, O. (1995), "Inertial properties in robotic manipulation: an object-level framework", *The International Journal of Robotics Research*, Vol. 14 No. 1, pp. 19-36.

Kim, J., Khosla, P. and Chung, W. (1992), "Static modeling and control of redundant manipulators", *Robotics & Computer-Integrated Manufacturing*, Vol. 9 No. 2, pp. 145-157.

Lay, D.C. (2005), *Linear Algebra and Its Applications*, Pearson-Addison Wesley, Boston.

Leylavi, A., Stefano, S. and Dario, M.P. (2016), "Bio-inspired kinematical control of redundant robotic manipulators", *Assembly Automation*, Vol. 36 No. 2, pp. 200-215.

Liegeois, A. (1977), "Automatic supervisory control of the configuration and behavior of multibody mechanisms", *IEEE Transactions on Systems, Man and Cybernetics*, Vol. 7 No. 12, pp. 868-871.

Lockwood, E. (1961), *A Book of Curves*, The Syndics of the Cambridge University Press, London.

Nakamura, Y., Hanafusa, H. and Yoshikawa, T. (1987), "Task-priority based redundancy control of robot manipulators", *The International Journal of Robotics Research*, Vol. 6 No. 2, pp. 3-15.

Nevins, J. and Whitney, D. (1977), "Research issues for automatic assembly", *IFAC International Symposium on Information-Control Problems in Manufacturing Technology, 17-20 Oct*, Vol. 10, *Pergamon Press, Tokyo*, pp. 15-24.

Ott, C. (2008), *Cartesian Impedance Control of Redundant and Flexible-Joint Robots*, Springer-Verlag, Berlin.

Ott, C., Roa, M.A., Schmidt, F., Friedl, W., Englsberger, J., Burger, R., Werner, A., Dietrich, A., Leidner, D., Henze, B., Eiberger, O., Beyer, A., Bauml, B., Borst, C. and Albu-Schaffer, A. (2017), "Mechanisms and design of DLR humanoid robots", in Goswami, A. and Vadakkepat, P. (Eds), *Humanoid Robotics: A Reference*, Springer Science+Business Media B.V., Berlin, pp. 1-26.

Petrovic, P.B. (1988), "Istrazivanje i razvoj sistema za adaptivno spajanje delova u montazi primenom robota", Master's thesis, Mechanical Engineering Faculty, University of Belgrade, Beograd.

Petrovic, P.B. and Lukic, N. (2017), "Configuration-based compliance control of kinematically redundant robot arm, part I-theoretical framework", *FME*, Vol. 45 No. 4, pp. 468-474.

Petrovic, P.B., Lukic, N. and Danilov, I. (2014), "Robot-assisted 3D medical sonography", Rodic, A., Pisla, D. and Bleuler, H. (Eds), *New Trends in Medical and Service Robots, Mechanisms and Machine Science*, Springer-Verlag, Berlin, pp. 45-61.

Salcudean, S., Bell, G., Bachmann, S., Zhu, W., Abolmaesumi, P. and Lawrence, P. (1999), "Robot-assisted diagnostic ultrasound-design and feasibility experiments", Taylor, C. and Colchester, A. (Eds), *Medical Image Computing and Computer-Assisted Intervention, Lecture Notes in Computer Science*, Springer, Berlin, pp. 1062-1072.

Salisbury, J. (1980), "Active stiffness control of a manipulator in Cartesian coordinates", *19th IEEE Int. Conference on Decision and Control, 10-12 Dec*, IEEE, *Albuquerque, NM*, pp. 95-100.

Sanan, S., Tully, S., Bajo, A., Simaan, N. and Choset, H. (2014), "Simultaneous compliance and registration estimation for robotic surgery", *Robotics: Science and Systems, 12-16 July, University of CA Berkeley*, pp. 1-9.

Siciliano, B. and Slotine, J.J. (1991), "A general framework for managing multiple tasks in highly redundant robotic systems", *Proceedings of the 5th International Conference on Advanced Robotics, 19-22 June, Pisa, Italy*, pp. 1211-1216.

Southern, W. and Lyons, C. (2002), "The study of a passive accommodation device in robotic insertion processes", *Journal of Materials Processing Technology*, Vol. 124 No. 3, pp. 261-266.

Svinin, M., Hosoe, S., Uchiyama, M. and Luo, Z. (2002), "On the stiffness and stiffness control of redundant manipulators", *IEEE International Conference on Robotics and Automation, 11-15 May, IEEE, Washington, DC*, pp. 2393-2399.

Vukobratovic, M. and Borovac, B. (2004), "Zero-moment point-thirty five years of its life", *International Journal of Humanoid Robotics*, Vol. 1 No. 1, pp. 157-173.

Wang, L., Sun, C., Tan, J., Zhao, B. and Wan, G. (2015), "Improvement of location and orientation tolerances propagation control in cylindrical components assembly using stack-build assembly technique", *Assembly Automation*, Vol. 35 No. 4, pp. 358-366.

Whitney, D. (1982), "Quasi-static assembly of compliantly supported rigid parts", *Journal of Dynamic Systems, Measurement, and Control*, Vol. 104 No. 1, pp. 65-77.

Yanai, H., Takeuchi, K. and Takane, Y. (2011), *Projection Matrices, Generalizes Inverse Matrices, and Singular Value Decomposition*, Springer, New York, NY.

Zhou, Z., Zhou, Y., Wang, N., Gao, F., Wei, K. and Wang, Q. (2014), "On the design of a robot-assisted rehabilitation system for ankle joint with contracture and/or spasticity based on proprioceptive neuromuscular facilitation", *IEEE International Conference on Robotics & Automation (ICRA), Hong Kong Convention and Exhibition Center, May 31 - June 7, IEEE, Piscataway, NJ*, pp. 736-741.

Corresponding author

Nikola Lukic can be contacted at: nlukic@mas.bg.ac.rs